Locomotor rhythm maintenance: electrical coupling among premotor excitatory interneurons in the brainstem and spinal cord of young *Xenopus* tadpoles

Wen-Chang Li, Alan Roberts and Stephen R. Soffe

School of Biological Sciences, University of Bristol, Woodland Road, Bristol BS8 1UG, UK

Electrical coupling is important in rhythm generating systems. We examine its role in circuits controlling locomotion in a simple vertebrate model, the young *Xenopus* tadpole, where the hindbrain and spinal cord excitatory descending interneurons (dINs) that drive and maintain swimming have been characterised. Using simultaneous paired recordings, we show that most dINs are electrically coupled exclusively to other dINs (DC coupling coefficients ∼8.5%). The coupling shows typical low-pass filtering. We found no evidence that other swimming central pattern generator (CPG) interneurons are coupled to dINs or to each other. Electrical coupling potentials between dINs appear to contribute to their unusually reliable firing during swimming. To investigate the role of electrical coupling in swimming, we evaluated the specificity of gap junction blockers (18-β-GA, carbenoxolone, flufenamic acid and heptanol) in paired recordings. 18-β-GA at 40–60 μM produced substantial (84%) coupling block but few effects on cellular properties. Swimming episodes in 18-β-GA were significantly shortened (to ∼2% of control durations). At the same time, dIN firing reliability fell from nearly 100% to 62% of swimming cycles and spike synchronization weakened. Because dINs drive CPG neuron firing and are critical in maintaining swimming, the weakening of dIN activity could account for the effects of 18-β-GA on swimming. We conclude that electrical coupling among pre motor reticulospinal and spinal dINs, the excitatory interneurons that drive the swimming CPG in the hatchling *Xenopus* tadpole, may contribute to the maintenance of swimming as well as synchronization of activity.

Abbreviations aIN, ascending interneuron; cc, cross-correlation; ce, coefficient; cIN, commissural interneuron; CPG, central pattern generator; dIN, descending interneuron; 18-β-GA, 18-β-glycyrrhetinic acid; FFA, flufenamic acid; hdIN, hindbrain decending interneuron; MN, motoneuron; R_{inp}, cellular input resistance; RMP, resting membrane potential; SSP, spontaneous synaptic potential; VR, ventral root.

The involvement of electrical coupling mediated by gap junctions in the oscillatory behaviour of vertebrate neuronal networks has been demonstrated in many systems including neocortex (Blatow *et al.* 2003), somatosensory cortex (Roopun *et al.* 2006), hippocampus (e.g. Draguhn *et al.* 1998; Traub *et al.* 2003), olfactory bulb (Friedman & Strowbridge, 2003), amygdala (Sinfield & Collins, 2006), the inferior olive nuclei (e.g. (Long *et al.* 2002; Leznik & Llinas, 2005), locus coeruleus (Christie *et al.* 1989; Alvarez *et al.* 2002; Ballantyne *et al.* 2004), respiratory brainstem (Rekling & Feldman, 1997; Rekling *et al.* 2000; Bou-Flores & Berger, 2001) and spinal cord (Tresch & Kiehn, 2000; Asghar *et al.* 2005). The established role of such coupling is to synchronize the neuronal

activity of the connected neurons (see reviews: Kiehn & Tresch, 2002; Connors & Long, 2004) but it may have other roles.

In vertebrate motor systems, electrical coupling is widespread. It has long been known electrical coupling exists between spinal cord motoneurons (Grinnell, 1966; Cullheim *et al.* 1977; Fulton *et al.* 1980; Westerfield & Frank, 1982; Walton & Navarrete, 1991; Perrins & Roberts, 1995*a*; Logan *et al.* 1996; Chang *et al.* 1999; Tresch & Kiehn, 2002). In the brainstem, electrical coupling between respiratory motoneurons has been documented (Mazza *et al.* 1992; Rekling & Feldman, 1997; Rekling *et al.* 2000). Structural evidence suggests that gap junctional connections between neurons are widespread in the
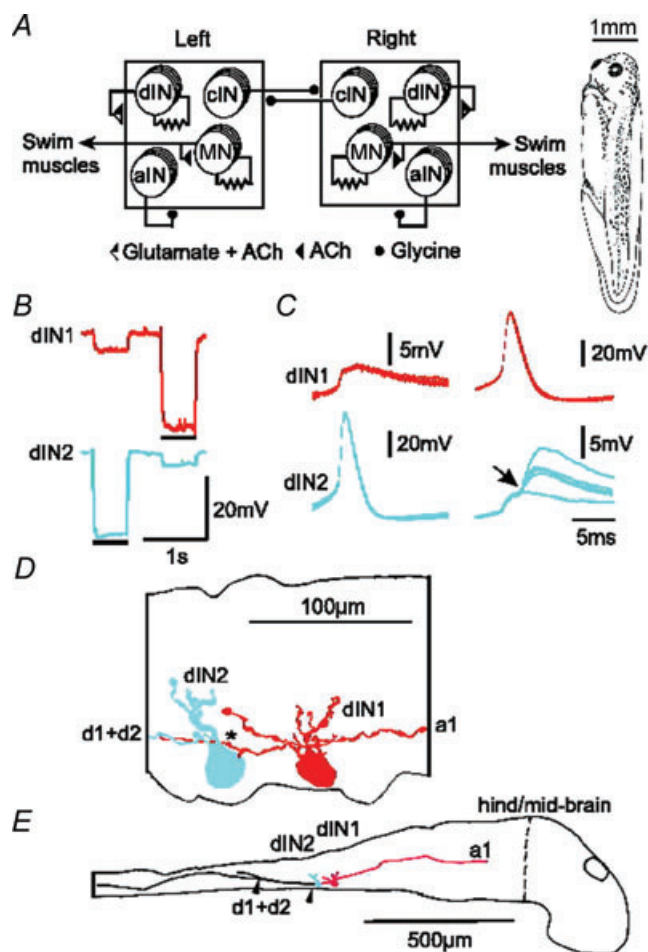
Figure 1. *Xenopus* tadpole, swimming CPG, and electrical coupling between dINs with their anatomy
A, the tadpole swimming CPG comprises half-centres on each side of the spinal cord (squares). Each half-centre has populations of cINs, aINs, dINs and MNs (more details in text). Filled circle connections are inhibitory and triangles are excitatory. Connections onto a half-centre affect all neurons in it. Resistor symbols indicate electrical coupling between MNs and between dINs. The drawing (right) shows the tadpole at developmental stage 37/38. *B–E*, paired recording of two dINs filled by neurobiotin. *B*, when either dIN was hyperpolarised by square pulse current injection (bars, dIN1: −70 pA, dIN2: −100 pA), a smaller response was seen in the other neuron. *C*, the shape of spikes evoked at the start of a step current injection into one dIN and the responses in the other. dIN2 makes electrical synapse onto dIN1. In contrast, dIN2 displayed EPSPs (arrow) superimposed on the electrical synaptic response evoked by dIN1 firing. The EPSPs were consistent in latency but variable in size indicating a monosynaptic chemical connection. Five traces overlapped. *D*, high power tracing shows dIN1 has both ascending and descending axons (red, a1, d1) but dIN2 only has a descending axon (blue, d2). The descending axon of dIN1 may contact the dIN2 soma and basal dendrite (*). *E*, low power tracing shows somata and descending axons closely apposed to each other for a distance of about 200 μm (between arrowheads). Vertical dashed line indicates the hindbrain/midbrain border which is set as 0 in longitudinal position measurements.

mammal spinal cord (Rash *et al.* 1996). Electrical coupling among several types of premotor interneuron has also been reported in different vertebrates but its role in system functions is often not clearly defined. In the lamprey spinal cord direct coupling between excitatory interneurons and motoneurons can contribute to motoneuron excitatory drive during swimming (Christensen, 1983; Parker, 2003). The electrically connected network of interneurons in young zebra fish embryo spinal cord was hypothesized to form an early scaffold for the development of locomotion rhythm generation circuits at later stages (Saint-Amant & Drapeau, 2001). Electrical coupling was also found between locomotor-related excitatory HB9 positive inter-neurons in newborn and juvenile mouse spinal cord, which may provide a mechanism of synchronizing their activity in locomotion (Hinckley & Ziskind-Conhaim, 2006). In the respiratory pre-Bötzinger complex, coupling between premotor interneurons was found (Rekling *et al.* 2000) and the coupling between rhythmogenic type-1 neurons was proposed to contribute to the control of respiratory frequency (Bou-Flores & Berger, 2001). The electrical coupling between inferior olive neurons was suggested to be essential for proper timing of their firing and cerebellar motor learning (Van Der Giessen *et al.* 2008). One of the clearest cases is found in the brainstem nuclei driving electric organ discharge in weakly electric fish. Here the pacemaker nucleus neurons are coupled (Moortgat *et al.* 2000*a*) to synchronize their discharge which drives reticulospinal premotor interneurons.

In this paper we ask whether electrical coupling between interneurons in a vertebrate locomotor network may have more significance than the simple synchronization of firing. We address this problem in the hatchling *Xenopus* tadpoles at stage 37/38 (Fig. 1*A*) because in this animal we have detailed information on the neuronal networks generating swimming locomotion. The tadpole can swim freely at frequencies of 10–25 Hz when the skin is briefly stroked or when the light is dimmed. This swimming activity involves alternating contractions of swimming muscles spreading from head to tail along the tadpole's trunk. The swimming CPG has been explored in studies on immobilised tadpoles and comprises four types of rhythmically active neurons (Fig. 1*A*, Roberts, 2000). Glycinergic commissural interneurons (cINs) send axons to the other side of spinal cord to inhibit all contralateral CPG neurons and therefore coordinate the alternating activity between the two sides. Glycinergic ascending inter-neurons (aINs) have ipsilateral ascending and descending axons feeding inhibition back to ipsilateral CPG and sensory pathway neurons (Li *et al.* 2002, 2004*a*). Many motoneurons have central axons which make cholinergic and electrical synapses onto nearby motoneurons (Perrins & Roberts, 1995*a*). Descending interneurons (dINs) have ipsilateral descending axons and excite all types of CPG neurons during swimming by coreleasing glutamate and

acetylcholine (Li *et al.* 2004*b*, 2006). Anatomically, dINs form a longitudinal column extending from the hindbrain into the spinal cord (Roberts & Alford, 1986). When we examined their properties and synaptic connections we did not find any consistent differences between the hdINs in the hindbrain (reticulospinal region) and dINs in the spinal cord except that more hindbrain neurons have an ascending as well as a descending axon (Li *et al.* 2006). In this paper, to simplify description and illustration and because the properties we describe were independent of location, we group these neurons together under the name of dIN.

We first describe electrical coupling within the dIN population and its properties. To investigate the role of this coupling we then evaluate the specificity of four candidate gap junction blockers that have been used elsewhere. Effective block of electrical coupling between dINs with one of these, 18-β-GA was associated with shortened swimming episodes following brief skin stimulation and decreased reliability of firing across the dIN population driving swimming. We conclude that, as well as synchronising neuronal activity, this electrical coupling may therefore influence the reliability of firing within a group of coupled neurons and in this way influence the ability of the locomotor system to sustain swimming episodes following stimulation.

Methods

Seventy *Xenopus* tadpoles at stage 37/38 (2 days old, Fig. 1A) were used in this study. Procedures for producing tadpoles using a *Xenopus* colony comply with UK Home Office Animals (Scientific Procedures) Act 1986 and have received local ethical approval. Tadpoles were immobilized in 10 μM α-bungarotoxin saline after brief anaesthesia with 0.1% MS-222 (Sigma, UK). Anaesthetics were not used during experiments because at stage 37/38 they are considered to be insentient.

Whole-cell recording methods have been slightly modified from those published previously (Li *et al.* 2002). Briefly, immobilized tadpoles were pinned in a bath of saline (concentrations in mM: NaCl 115, KCl 3, CaCl$_2$ 3, NaHCO$_3$ 2.4, Hepes 10, adjusted with 5 M NaOH to pH 7.4). Dissections were made to remove skin and muscles over the left side of the hindbrain and spinal cord and the yolky belly beneath the exposed CNS and muscles. A dorsal cut was made along the spinal cord to open the neurocoel. In experiments where swimming activities were monitored, cuts were made in the wall of the neurocoel on the right side to expose the ventrally located neurons. In many other experiments, the left side of the caudal hindbrain and spinal cord were also removed to improve visibility and accessibility. After dissection the tadpole was re-pinned in a small 2 ml recording chamber with

saline flow of about 2 ml min^{-1}. Exposed neuronal cell bodies were seen using a $\times$40 water immersion lens with bright field illumination on an upright Nikon E600FN microscope. Gap junction blockers were applied by switching the perfusion tube from the control 100 ml stock saline bottle to a similar bottle containing 18-β-glycyrrhetinic acid (18-β-GA), carbenoxolone, flufenamic acid (FFA) (Sigma) or heptanol (Fluka).

Whole-cell current clamp recordings were made from exposed neuronal cell bodies following the dissections. Patch pipettes were routinely filled with 0.1% neurobiotin and 0.1% Alexa Fluor 488 (Molecular Probes, Eugene, OR, USA) in the intracellular solution (concentrations in mM: potassium gluconate 100, MgCl$_2$ 2, EGTA 10, Hepes 10, Na$_2$ATP 3, NaGTP 0.5 adjusted to pH 7.3 with KOH) and had resistances ranging from 10 to 20 MΩ. Tip potentials were corrected before making recordings. Tadpole fictive swimming was started by applying a 1 ms electrical pulse to tadpole skin via a suction electrode or briefly dimming the microscope illumination. To improve success rate of recording pairs of dINs, extracellular loose-patch recordings were made beforehand to screen them. This was done by starting fictive swimming activities in the network and visually inspecting the shape of extracellular action potentials of rhythmic neurons recorded in loose-patch mode using the whole-cell recording pipettes filled with intracellular solution. dINs/hdINs fire one spike reliably on each swimming cycle (Li *et al.* 2006) and their extracellular spikes are wide and lack AHP-like potentials. In contrast, other types of CPG neurons may fire more than 1 spike per cycle occasionally or fail to fire spikes on some swimming cycles. Their extracellular spikes are narrow and normally possess a clear AHP-like phase. Fictive swimming activity was monitored using another suction electrode placed on the muscle cleft to record ventral root (VR) discharges. Signals were recorded with an Axoclamp 2B (Axon Instruments, Union City, CA, USA) in conventional bridge mode, acquired with Signal software through a CED 1401 Plus interface (Cambridge Electronic Design, Cambridge, UK) with a sampling rate of 10 kHz. Offline analyses were made with Minitab and Excel. All values are given as means $\pm$ S.D.

Neuronal anatomy was normally checked after recording using a fluorescence attachment, and then specimens were fixed and processed as described previously (Li *et al.* 2002). The location of recorded neurons in live animals was drawn schematically during experiments and confirmed by later neurobiotin staining. Final anatomical tracings were made using a drawing tube at times 100 and 1000 on a bright field microscope. For some neurons optical sections were photographed and reassembled in Photoshop. Neurons were identified by their specific anatomy (Roberts & Clarke, 1982; Li *et al.* 2001). The distance between the recorded neurons was measured using a small

mechanical micrometer attached to the microscope translation table during recording and/or on the drawing after processing.

Results

All dINs were recorded in the caudal hindbrain and rostral spinal cord area (0.3–1 mm from the mid-hindbrain border). They were identified based on their descending axon projection revealed by fluorescence imaging and neurobiotin staining, and by their characteristic, long-duration action potential evoked by current injection

Figure 2. The properties of electrical coupling between pairs of dINs

A, scatter plot of coupling coefficients. Negative-current test pulses were injected into the rostral dIN (R-C) or the caudal dIN (C-R). Regression: $y = 1.7 + 0.91x$ ($R^2 = 0.63$, $n = 55$, $P < 0.001$). *B*, coupling coefficients (average of both directions for each dIN pair) decrease with the distance separating the two dIN somata (regression $y = 10.3 - 0.03x$, $R^2 = 0.13$, $n = 31$, $P = 0.049$). *C*, examples of responses of dIN2 to sinusoidal current injection into dIN1 at 3 and 30 Hz, respectively. *D*, the dependency of electrical coupling coefficient on the frequency of injected sinusoidal current (mean ± S.D., $n = 5$ dINs). *E*, paired recording showing that attenuation between electrically coupled dINs is greater for spikes than for sustained depolarisation. Injection of current (cur) into dIN2 depolarises the cell and evokes a single spike, producing a depolarisation and spikelet in the electrically coupled dIN1 (left and middle). Spikes in dIN1 produce similar spikelets in dIN2 (right). In this example there is no chemical synaptic interaction.

or during their reliable firing in fictive swimming (see Fig. 1 of Li *et al.* 2006). In all the paired whole-cell recordings where synaptic actions were found (34/55, 62%), stimulating one dIN evoked EPSPs (Fig. 1*C*) in the other dIN, confirming that these dINs were excitatory.

Electrical coupling between excitatory premotor interneurons

Electrical coupling between pairs of recorded dINs was tested by injecting 500 or 600 ms hyperpolarizing current pulses into one neuron and monitoring the membrane potential changes during the current injection in the other neuron. Where coupling existed, a small hyperpolarization with the same on and off times as the current injection was measured relative to the neuron's resting membrane potential (RMP; Fig. 1*B*).

Recordings from random pairs of dINs showed that 90% of dINs were electrically coupled to the other recorded dINs (55/61 pairs) regardless of their longitudinal locations. However, there was little evidence of dye-coupling. In 78 out of 83 individual dINs where electrical coupling was found with other dINs, only the recorded dINs which were filled with neurobiotin were labelled (Fig. 1*D* and *E*); no additional neurons showed labelling. In the remaining five dINs, four were dye-coupled to a second neuron and one was coupled to two additional neurons revealed by neurobiotin staining. Because the staining of these coupled cells was very faint, it was difficult to identify them anatomically. However, since we have only found coupling among dINs themselves, it is likely that they were also dINs.

In 27 animals where only one pair of electrically coupled dINs was filled with neurobiotin and their anatomy was clear, we tried to resolve the location of electrical coupling contacts. In six cases the dINs were adjacent and their dendrites overlapped. In all cases there was potential contact where at least one dIN axon appeared to contact the other coupled neuron on: soma (4 pairs); basal dendrites $<10 \mu m$ from the soma (22 pairs); dendrites further from soma (4 pairs). In 20 pairs, the dIN axons tightly intermingled with each other and it was difficult to resolve individual axons (Fig. 1*D* and *E*). Since dINs also make chemical synapses with each other (Li *et al.* 2006), any contacts may contain both chemical and electrical synapses (Fig. 1*C*). The anatomy suggests that dendrite to dendrite contacts are uncommon, so electrical coupling could occur mainly at axon to dendrite or axon to axon contacts.

We then tested the properties of dIN to dIN electrical coupling. All coupling was bi-directional. Coupling coefficients (the voltage response in the uninjected neuron expressed as a percentage of the voltage response in the injected neuron; Fig. 2*A*) showed the coupling to
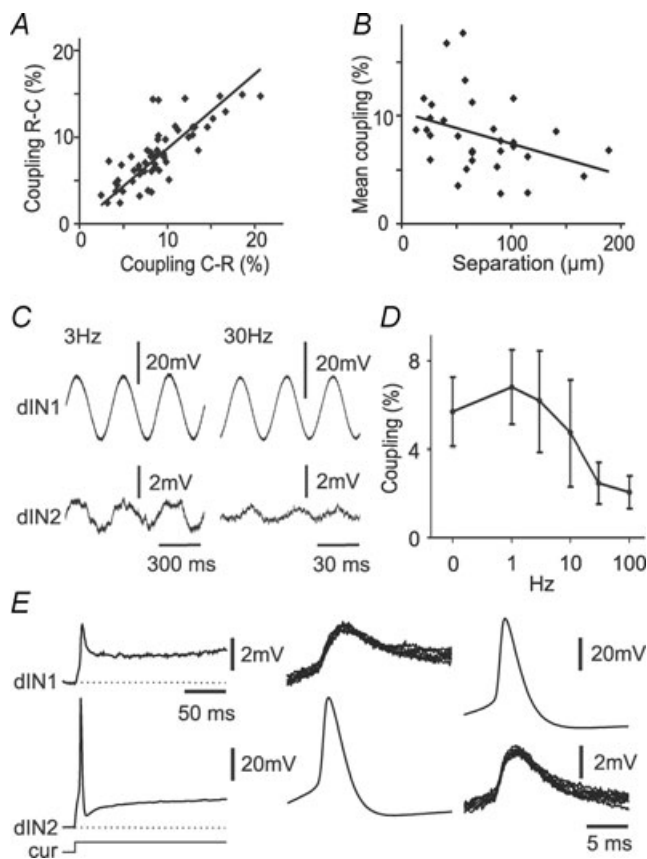
be slightly stronger from caudal to rostral ($9 \pm 3.9\%$) than in the opposite direction ($8 \pm 3.4\%$, paired *t*-test, $n = 55$ neuron pairs, $P = 0.004$). The distance measured between the centres of two coupled dIN somata ranged from 13 to 189 μm (72 ± 43 μm, $n = 31$). The distances between dIN pairs without electrical coupling was not significantly longer (77, 115, 166 μm in 3 pairs, $P = 0.22$, *t*-test). Coupling coefficients between dINs decreased with distance (Fig. 2*B*). The filtering properties of the coupling were examined using sinusoidal current injection into one dIN at different frequencies (Fig. 2*C* and *D*; $n = 5$ pairs). Coupling decreased markedly at frequencies above around 10 Hz.

One consequence of the filtering properties of the coupling between dINs was that spikes were relatively strongly attenuated compared to responses to injected DC (Fig. 2*E*). Impulses in individual dINs would be expected to produce spikelets (action potentials attenuated by the low-pass filtering properties of the electrical junctions) in neighbouring dINs to which they are electrically coupled. Individual spikelets were generally hard to distinguish during swimming, but were seen in paired recordings between dINs where there was electrical coupling but no additional chemical synaptic connection (see above), and the presynaptic cell was made to fire. Typically, these unitary spikelets were ~1–2 mV in amplitude (Fig. 2*E*), suggesting a coupling coefficient of <3%, contrasting with the larger DC coupling described above (8–9%).

In contrast to the coupling found between dINs, no clear electrical coupling was found in 39 pairs where a dIN was recorded with another type of CPG neuron (25 motorneurons, 7 cINs and 7 aINs) apart from weak coupling in two of the dIN-motoneuron pairs (coefficients were 2.1% and 4.7%, respectively). There was also no coupling found between ipsilateral aINs ($n = 16$ pairs) or cINs ($n = 28$ pairs), or between aINs and cINs ($n = 28$ pairs). Among premotor interneurons involved in swimming, electrical coupling therefore seems to be almost exclusively between dINs.

Electrical coupling during fictive swimming

During swimming, dINs typically fire a highly reliable single spike on each cycle, in phase with ipsilateral ventral root discharge (termed 'on-cycle' timing; Fig. 3*A*; Li *et al.* 2006). The high probability of electrical coupling between dINs and their near-synchronous firing during swimming made it likely that spikelets from coupled neurons (described above) should summate in individual dINs. We therefore looked for evidence that the electrical coupling among dINs contributes to their firing in swimming.

Hyperpolarizing current was injected into interneurons during swimming to block action potentials and reveal the underlying on-cycle excitation, which consists of phasic, chemical EPSPs and any electrically coupled

potentials (arrowhead, Fig. 3*B*). dINs often still fired when hyperpolarised (Fig. 3*B*) and such spikes were significantly delayed (by 5.9 ± 2.1 ms for spikes in 10 dINs; $P < 0.001$, paired *t* test). The spikes rode the on-cycle PSPs which were revealed when spikes failed (Fig. 3*B* and *C*). In some cases, delayed spikes appeared on the falling phase of the EPSP (Fig. 3*C*) suggesting a distant site for initiation. In contrast, spikes in other interneurons which are not electrically coupled (aINs and cINs) were either unreliable (Fig. 3*D*) or easily blocked by hyperpolarisation (not illustrated).

To investigate whether the electrical coupling between dINs contributes to their reliable firing, we first compared estimates of firing thresholds at rest and during swimming for the three types of interneurons. As an estimate at rest, we used the level of depolarisation produced by the strongest injected current that did not produce firing. As an equivalent estimate during swimming, we used the peak depolarisation of the on-cycle PSPs that underlie spiking. This was measured for ten cycles where spiking failed, when firing was adjusted by current injection to ~50% of swimming cycles (Fig. 3*B*). Estimated firing thresholds from rest were similar in all three neuron types (Fig. 3*E*; 10 aINs: -29.4 ± 5.4 mV; 10 cINs: -27.1 ± 5.1 mV; 16 dINs: -27.1 ± 3.9 mV; $P > 0.2$). During swimming, estimated firing thresholds for aINs and cINs were slightly more negative than their values from rest (Fig. 3*D*,*E*; 10 aINs: -34.4 $\pm$ 3.6 mV; 10 cINs: -33 ± 3.9 mV: $P < 0.05$). In contrast, the estimated firing thresholds in 14 dINs (-45.2 ± 9.5 mV) were significantly more negative during swimming than their levels at rest ($P < 0.001$), and the thresholds for aINs and cINs during swimming ($P < 0.001$, ANOVA, Fig. 3*E*). This meant that the spikes that persisted in hyperpolarised dINs could not have been initiated close to the recordings site by the on-cycle excitation as this peaked well below the dIN firing threshold (Fig. 3*B* and *C*).

Hyperpolarization of firing thresholds during fictive locomotion was observed in adult cat hindlimb motoneurons (Krawitz *et al.* 2001). Modelling suggested that a modulated hyperpolarization of the voltage dependency of fast sodium channels in the axon hillock could lead to such a phenomenon (Dai *et al.* 2002). However, here we propose that the firing of hyperpolarised dINs is likely to be a consequence of electrical coupling at relatively distant sites on the axon, as suggested by the anatomy (see above). Summation of spikelets at such distal axonal coupling sites could evoke spikes that would propagate antidromically to the soma, but would be difficult to suppress by current injected at the soma and would be delayed, just as we observed. Additional support comes from recordings of three further dINs in which injection of negative current, to block spikes, revealed the usual on-cycle PSPs on some cycles, but significantly larger on-cycle depolarisations on other cycles (Fig. 3*F*; mean amplitude differences were 29.9, 30.5

and 34.7 mV, respectively; $P < 0.001$ in each case). We interpret these larger, later (Fig. 3*G*, red traces) on-cycle potentials again as active antidromic spikes, but in this case prevented from invading the recording site by the injected hyperpolarising current. The variable timing and occurrence but relatively large and constant amplitude of these larger potentials makes it highly unlikely that they are simply summated spikelets from other dINs. For all three dINs described here, the anatomy was typical. The dendrites were short ($<115\,\mu$m), and the thin axon ($<0.5\,\mu$m) arose directly from the soma. We would

therefore expect hyperpolarisation at the soma to provide effective control of the membrane potential of soma and dendrites, and therefore prevent invasion of full spikes, but be less able to prevent initiation of antidromic spikes more distally.

We conclude that dIN spikes can be driven by on-cycle excitation, like other swimming CPG neurons. However, if the on-cycle excitation is insufficient to drive firing, their widespread electrical coupling allows summation of spikelets resulting from spikes in other dINs to still initiate spikes distal to the soma. Electrical coupling between dINs
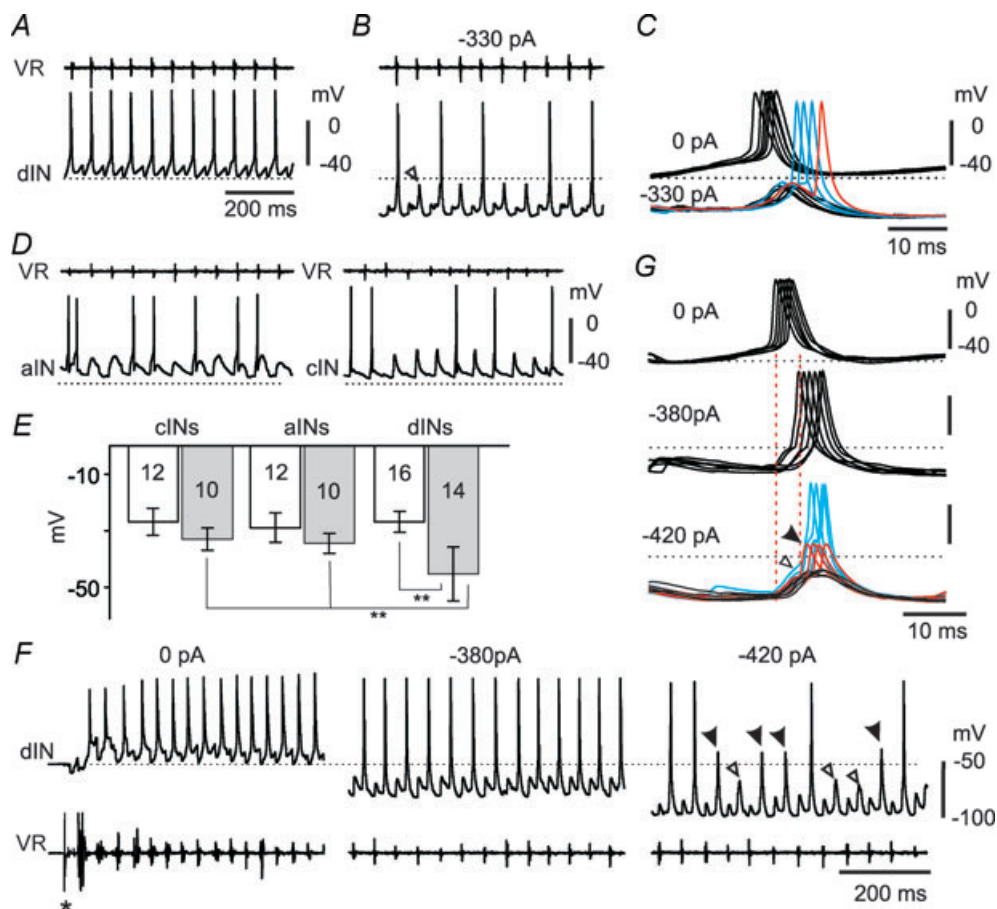

Figure 3. Electrical coupling and dIN firing during swimming
A, recording of activity in a dIN during swimming, monitored with a ventral root recording on the same side (VR). The dIN fires reliably on each cycle. *B*, hyperpolarisation to reduce firing to ~50% of cycles reveals underlying 'on-cycle' excitation (open arrowhead) whose peak does not even reach the resting potential (dotted line). *C*, at an extended time scale, impulses remaining during hyperpolarisation are delayed and can arise from the falling phase of the underlying excitation (e.g. red trace). *D*, swimming recorded in an aIN and a cIN where firing is occurring on ~50% of cycles. Spikes fail while the underlying on-cycle excitation is still substantially above the resting potential. VR in cIN was recorded from the opposite side. *E*, estimates of firing threshold at rest (open bars) and during swimming (grey bars) for three interneuron types. Neuron numbers are indicated (**$P < 0.001$). *F*, a dIN again firing reliably during swimming; initiated by a short current pulse to the skin (*); monitored by VR on the opposite side. Reliable firing continues even with −380 pA current injected into the dIN. When the hyperpolarising current is increased to −420 pA, firing starts to fail and reveals the underlying on-cycle excitation on some cycles (open arrowheads), and all-or-none, probable axonal action potentials on others (filled arrowheads; see text). *G*, overlapped spikes from *F*, (synchronised to VR burst onset). Injection of −380 pA delays the spikes. Injection of −420 pA causes some spike failure revealing small, early-onset potentials (black = synaptic excitation: open arrowhead) and larger, later-onset potentials (red = axonal action potentials: filled arrowhead) which are delayed like the remaining full spikes (blue). Dotted lines represent the resting potential in all cases.

will therefore play a significant role in maintaining the high reliability of firing within the dIN population.

## The effects of blockers on electrical coupling between dINs

Our evidence suggests that electrical connections between dINs could contribute to the reliable firing of the dIN population during swimming. To try to test the consequences of this for maintenance of the swimming pattern, we wished to alter the electrical coupling between dINs by using gap junction blockers. Despite the shortcomings of existing gap junction blockers (see below) we considered this worthwhile because, as shown above, coupling among premotor interneurons is virtually exclusive to dINs making it feasible to target these connections directly. Additional electrical coupling described between homonymous spinal motoneurons (Perrins & Roberts, 1995b) must have little or no effects on maintenance of the swimming rhythm because swimming is not significantly affected by removing the majority of the spinal cord, i.e. the part caudal to the 3rd post-otic myotome segment (Li et al. 2006). Although different gap junction blockers, especially carbenoxolone and its derivatives have been used previously in many studies (for recent examples, Blenkinsop & Lang, 2006; Urbano et al. 2007), all of them have been shown to have some non-specific effects (Rozental et al. 2001; Rouach et al. 2003; Srinivas & Spray, 2003; Leznik & Llinas, 2005; Wang

et al. 2006), making their influence hard to interpret at the system level. In order to investigate whether blocking electrical coupling could affect swimming activity by changing the reliability of dIN firing, we took two measures to minimise the interference of non-specific effects. Firstly, we investigated four reported gap junction blockers in paired recordings to identify the one with the least non-specific effects in the tadpole system. In particular, we looked for direct effects of the blocker on dIN firing or synaptic output. Secondly, we analysed effects of our selected blocker on the swimming pattern and on the activity of dINs during swimming while using paired recordings to directly monitor changes in coupling strength. This allowed us to use cross-correlation analysis of time series measurements to identify effects that significantly tracked changes in coupling strength.

We first examined the effectiveness of heptanol, FFA, carbenoxolone and 18-β-GA on electrical coupling. Heptanol (2 mM) did not produce an obvious block, and carbenoxlone at concentrations of 100–300 μM only resulted in weak block (<50%), up to 30 min after application. Considering also their fast-occurring, non-specific effects (see below), we rejected these two blockers and concentrated instead on FFA and 18-β-GA. Both FFA (100–400 μM, Fig. 4) and 18-β-GA (40–60 μM; Fig. 5) led to near-complete block of the electrical coupling between dINs (reduction to 21.1 ± 9 and $15.6 \pm 5.6\%$ of control respectively, both $n = 6$). At these concentrations, the time to reach stable block was much quicker for FFA

Figure 4. The effects of gap junction blockers on dIN properties 5–10 min after their application

A, an example dIN pair where 200 μM FFA was applied. After 5 min the RMP (control level shown as a dotted line) became more negative in both dINs (arrowed) and there was a dramatic increase in SSP frequencies in dIN2. After 12 min in wash, both effects disappeared. There was a small increase in R_{inp} in both neurons. Current injection was −100 pA in dIN2 in FFA and Wash and −120 pA in both dINs in other cases. B, summary of effects of four gap junction blockers on RMP, spike height, R_{inp} and SSP frequency (measured when RMP was hyperpolarized and all synaptic potentials appear depolarizing) within 5–10 min of blocker application. Numbers in brackets are the number of dINs analyzed for each measurement. Significance is indicated at $P < 0.05$ (*) or $P < 0.01$ (**; paired t-test). Open bars are control. Grey bar measurements were made 5–10 min after application of heptanol (Hep; 2 mM), carbenoxolone (Carb; 100–300 μM), FFA (100–400 μM), or 18-β-GA (40–60 μM). Error bars represent S.D.
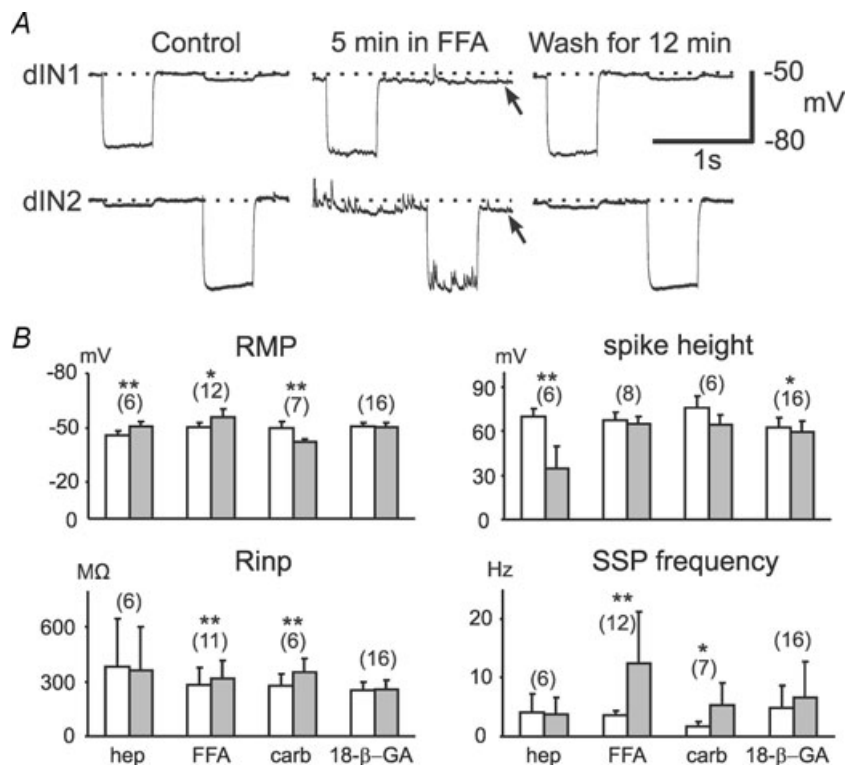
than 18-β-GA (5 ± 3 min and 35 ± 7 min respectively, both $n = 6$). Despite this difference, FFA and 18-β-GA increased cellular input resistance (R_{inp}) significantly by a similar amount (292 ± 101 to 345 ± 108 MΩ, $P = 0.002$, $n = 11$, 16% and 252 ± 46 to 298 ± 56 MΩ, $P = 0.02$, $n = 16$, 18%, respectively; measured once the block had stabilised). The similarity in the R_{inp} increase in both cases is expected if blockage of electrical coupling is the common mechanism.

We then assessed side-effects. Since electrical coupling block was slow to establish in most cases, we interpreted any changes in cellular properties occurring prior to this, in the first 5–10 min of application, to indicate side-effects
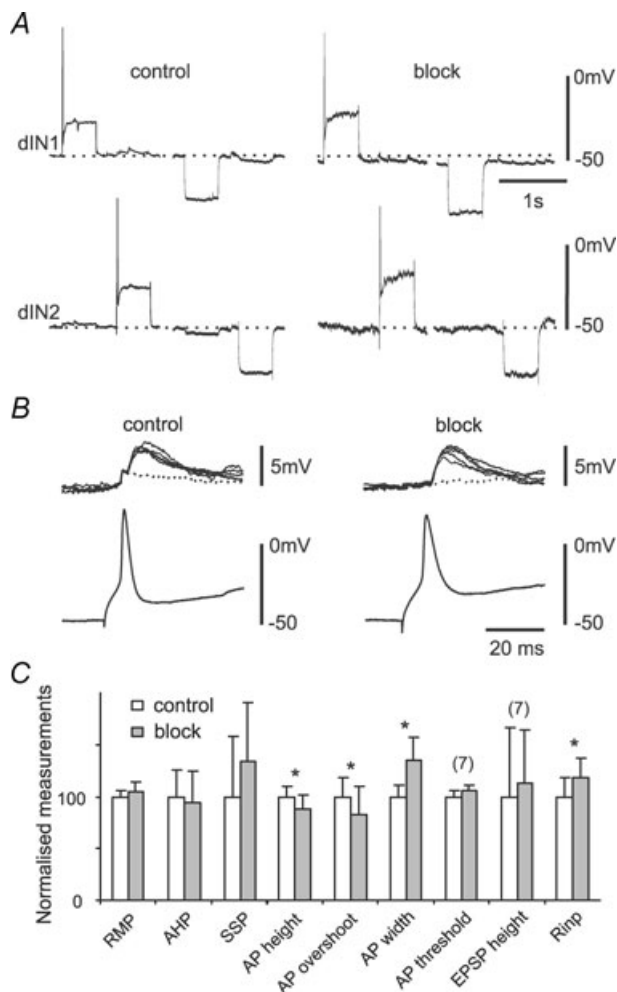

Figure 5. The effect of 18-β-GA on dIN properties after the block had established
A, a dIN's responses to positive and negative current injection in control and 40 min after 18-β-GA application. *B,* overlapped unitary EPSPs evoked by dIN firing in control and after the 18-β-GA coupling block had stabilised. The dotted traces are records where EPSP failed. Note the disappearance of the spikelet (Fig. 2*E*) in block. *C,* comparison of dIN properties in control and 18-β-GA block. AP is action potential and AHP is afterhyperpolarization ($n = 16$ dINs unless indicated). Error bars represent s.d.

rather than consequences of the block. The properties measured included: RMP, the height of action potentials evoked by current injection immediately above firing threshold, R_{inp}, and the frequency of spontaneous synaptic potentials (SSPs). Heptanol (2 mM) and carbenoxolone (100–300 μM) produced significant changes in some parameters, which must have been non-specific since neither blocked electrical coupling. The relatively rapid block of electrical coupling produced by FFA made it harder to assess the cause of other changes, and could have explained its effect on R_{inp}; however, changes in RMP and SSPs were more likely to have been side-effects (Fig. 4). The only change produced by 18-β-GA prior to blocking electrical coupling was a small reduction of spike height. Similar tests of 18-β-GA's effects on RMP, R_{inp}, SSP frequency and spike height 5–10 min following its application in seven inhibitory interneurons also revealed a 7.2% reduction in spike height (paired *t*-test, $P = 0.047$) and but no change in the other three measurements.

Because 18-β-GA seemed the best candidate gap junction blocker, we next investigated changes occurring after electrical coupling block had stabilised, to try to identify any that were likely to be non-specific effects rather than consequences of the block ($n = 8$ dIN pairs; Fig. 5). There was still no significant change in dIN RMP, spike AHP or SSP frequency. There were small but significant changes in spike shape: spike heights decreased from 64.9 ± 6.5 to 57.3 ± 7.8 mV ($P = 0.026$); overshoots were reduced from 25.7 ± 4.7 to 21.3 ± 4.7 mV ($P = 0.02$); width increased from 2.0 ± 0.2 to 2.7 ± 0.6 ms at 0 mV ($P = 0.002$; all paired *t*-tests, $n = 16$ neurons). However, dIN spikes are particularly variable in shape compared with other CPG neurons in the tadpole; a decrease in spike height/overshoot is typically associated with an increase in spike width (authors' unpublished observation). Also, dIN spike heights measured 5–10 min after 18-β-GA application were not significantly different from the ones measured after the block stabilised (on average after 35 min, see below; $n = 16$, paired *t*-test, $P = 0.06$). More importantly, these changes in spike shape were not associated with a change in the size of unitary EPSPs produced by seven of the dINs in the paired recordings (paired *t*-test, $P = 0.85$, Fig. 5*B*) or their spike thresholds (*t*-test, $n = 7$ dINs in control and block, $P = 0.25$). We do not know what mechanism produced the changes in spike shape, though we assume it was the same as produced the pre-block reduction in height (see above). However, the measurements show that neither the ability of dINs to fire spikes nor their synaptic output, either of which could affect the swimming pattern, was significantly altered by 18-β-GA application. Overall, 18-β-GA combined effective coupling block with the least non-specific effects of the four candidate blockers investigated and we selected this for our further investigations.

Gap junction blockers applied intracellularly can also sometimes block electrical coupling (Zsiros *et al.* 2007). We applied 18-β-GA (40 to 400 μM, $n = 3$ dIN pairs) and carbenoxolone (400 μM, 1 dIN pair) through the recording pipette. Diffusion of the blockers for up to 40 min failed to block the electrical coupling between dINs in all cases.

Effects of gap junction blockers on fictive swimming activity

Having identified 18-β-GA (at 40 μM) as able to provide effective block of electrical coupling, while having minimal side effects, we now tested its influence on the swimming pattern. The dINs drive all the CPG neurons in tadpole swimming and are also responsible for maintaining swimming (Li *et al.* 2006). Our evidence now suggests that their electrical coupling contributes to their reliable firing during swimming and we would expect this to play a significant role in the production of maintained swimming activity. Our approach was to monitor the time course of electrical coupling block by 18-β-GA between dIN pairs and, in the same recordings, identify changes in properties of the swimming rhythm and features of dIN activity that track the change in coupling strength. Although not confirming a causal link, this would show a significant relationship between electrical coupling strength and the nature of the swimming pattern. We made a detailed analysis of recordings from 6 dIN pairs in which the electrical coupling was blocked significantly.

We first looked at the time course of 18-β-GA's block of electrical coupling. To obtain averaged measurements across all six paired recordings, we divided the period following the onset of 18-β-GA application (at time = 0) in each paired recording into three regions: no detectable block, progressive block, and stabilised block. We then fitted linear regression lines to each region. The time at which electrical coupling started to be blocked was taken as the intersection of the first two lines; the time at which block stabilised was taken as the intersection of the second and third lines (Fig. 6*A*). Coupling coefficients were then normalised as percentages of the mean control coupling coefficients for each pair. Normalised measurements in all six recordings were grouped and averaged using 100 s bins to produce average time-series plots for cross-correlation analyses (see below). On average, it took 13.9 ± 5.7 min (range: 7.5–23.3) for the block to be first detected. A further 20.6 ± 5.6 min (range 15.1–28.2) was needed for the block to reach a stable final level ($n = 6$, Fig. 6). The average time from 18-β-GA application to stable block was therefore 34.5 ± 6.6 min (range: 24.4–42.3, Fig. 6*B*). By the time stable block was achieved, the average coupling coefficients dropped to $15.6 \pm 5.6\%$ of the initial levels (range: 8.9–22.4%).

Having used the paired recordings to directly monitor the time course of electrical coupling block for each neuron

pair, we then examined how swimming parameters changed during 18-β-GA block. Shortly (<10 min) after 18-β-GA application, spontaneous fictive swimming episodes started to occur. Spontaneous swimming disappeared after about a further 5–10 min of 18-β-GA
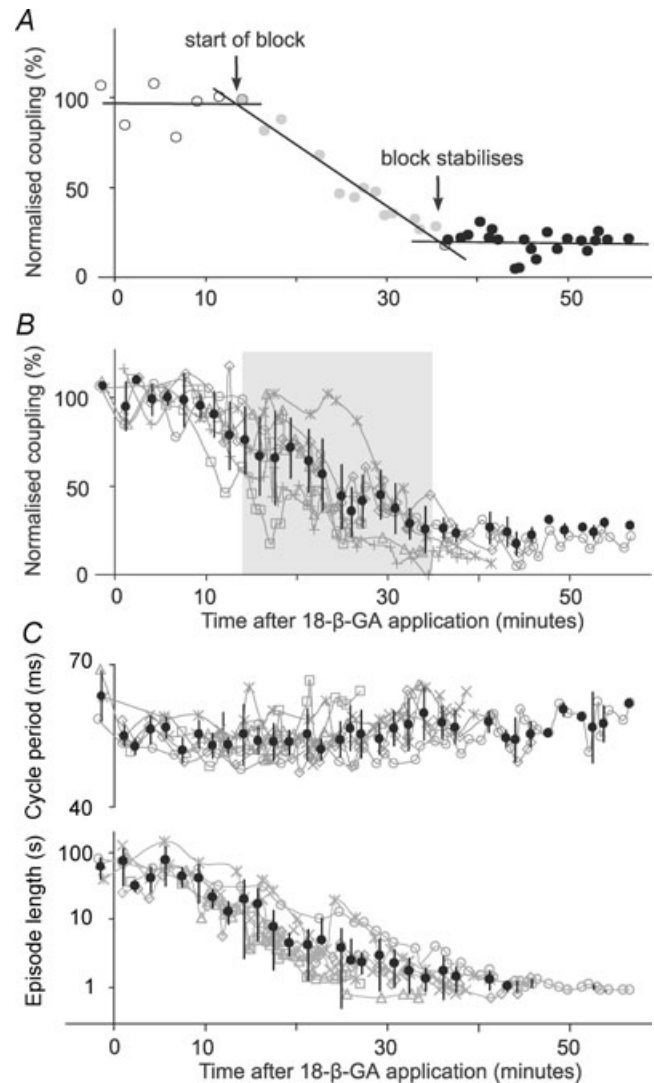

Figure 6. Time course of electrical coupling block by 18-β-GA (40 μM; applied at time = 0) and swimming pattern changes
A, determination of the time course of coupling block by 18-β-GA in a single example. Data points were chosen to give near-horizontal regression lines at the start and end (open circles: $y = -0.0007x + 96.827$, $R^2 = 0.0005$, and filled circles: $y = -0.0012x + 22.65$, $R^2 = 0.0044$, respectively). Data points in the middle as block progresses were fitted with a third line (grey circles: $y = -0.0573x + 142.93$, $R^2 = 0.9496$). The times when block starts (13.4 min) and stabilises (35.9 min) are given by the intersection of regression lines (see text for more details). *B*, time series of normalised electrical coupling strength measurements in 6 dIN pairs. Grey shading is between the mean times for the block to be detected and to reach stable block, respectively. *C*, time series of normalised swimming cycle period and episode lengths in the 6 paired dIN recordings. Grey swimming plots are data for individual recordings and black ones are averaged measurements (mean ± s.d.).

application and then skin stimuli were again needed to start fictive swimming. After the electrical coupling block had stabilised, the length of evoked swimming episodes decreased significantly from 57.7 ± 29.3 ($n = 24$ episodes) to 1.1 ± 0.3 s ($n = 46$ episodes; $P < 0.001$, 6 tadpoles, t-test; Fig. 6C). There was also a small increase in swimming cycle period (control: 55.4 ± 3.2 ms, $n = 22$ episodes, block: 58.5 ± 3.6 ms, $n = 46$ episodes, t-test, $P < 0.001$, Fig. 6C). Ventral root burst durations, measured at the tenth swimming cycle in each episode, increased with electrical coupling block (data not shown).

Having established that 18-β-GA application produces significant effects on the swimming pattern, we lastly inspected changes in different features of dIN activity following 18-β-GA application and their individual time courses. The first change in dIN activity was that by the time the electrical coupling block reached its maximum (and swimming episodes had shortened to about 1–2 s, see above) many dINs had lost their ability to fire spikes reliably during swimming (Fig. 7). In control, dINs fire typically one wide spike on each swimming cycle very reliably throughout each swimming episode (Figs 3A and F, and 7A). Firing reliability was measured as the percentage of swimming cycles where dINs fired spikes in each swimming episode. Occasionally, at the beginning of swimming episodes, depolarization of dIN membrane potential appeared to be sustained at about -5 mV and at this time, when network excitability is presumed to be at its highest, it was very difficult to identify spikes. In these cases, the beginning of the episodes was excluded. Overall in 18-β-GA, dIN firing reliability dropped from $99.5 \pm 2\%$ in control to $62 \pm 35\%$ when coupling was stably blocked (16 dINs: 12 from the 6 pairs, 4 from further dIN recordings, Fig. 7D and E, paired t-test, $P < 0.001$). However, the data suggested that dIN responses to 18-β-GA application may fall into two groups: at the end of application 10/16 dINs still fired spikes on most cycles ($86.7 \pm 13.6\%$) despite some drop-out during progression of the block (Fig. 7B), while in the other six dINs, firing became very unreliable and often failed ($21.1 \pm 14.1\%$, Fig. 7D and E). As described above, these changes in reliability occurred without any change in firing threshold at rest.

The second change following 18-β-GA application was that the dINs that continued to fire reliably in swimming fired less synchronously. Four of these dINs were recorded in two paired recordings (Fig. 8) and their firing was inspected in more detail. The time difference between the spikes of each dIN pair on the same swimming cycles were measured where spike trajectory reached -5 mV. In both paired recordings, the time difference was more variable during stable electrical coupling block. There was an increase in the standard deviation of the time differences (2.6 to 5.8 ms, and 1 to 3.4 ms, $n > 40$ cycles in each case, Fig. 8). Block of electrical coupling therefore appears to
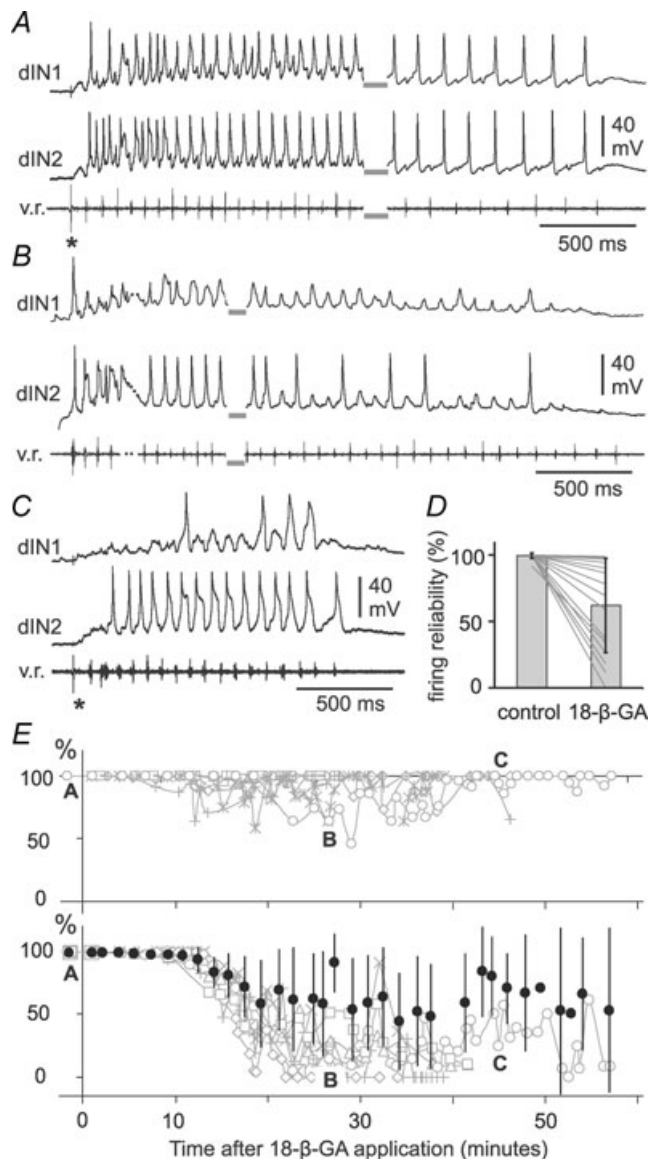

Figure 7. The reliability of dIN firing following 18-β-GA application

A, 2 dINs show typical, reliable, 1 spike per cycle firing in swimming before 18-β-GA application. Swimming was started by electrical stimulation on the skin (*) and lasted for 93 s (grey bars show the break in recording). There is a typical swimming frequency drop from the beginning to the end of the episode. B, while the coupling block is progressing (44% of control), dIN1 only fires 1 spike while dIN2 still fires on the majority of swimming cycles. Swimming was spontaneous and just the start (dots indicate a brief sampling gap) and the end are shown (grey bars show the break in recording). C, when the 18-β-GA block is stable (12% of control), the swimming episode (started by skin stimulation at *) is shortened to ~1.3 s. dIN1 fires 3 spikes while dIN2 still fires very reliably. D, summary of the changes in firing reliability of 16 dINs in 9 animals before block and in final 18-β-GA block. Lines indicate changes in individual neurons. E, time series plots of firing reliability (%) for 12 dINs in 6 paired recordings. Grey curves and symbols in the upper panel are 6 dINs which fired reliably throughout 18-β-GA application. Reliability for 6 dINs in the lower panel dropped gradually and then stayed at low levels. Filled symbols show averaged time series of firing reliability of all 12 dINs (mean ± s.d.). The time for the episodes illustrated in A, B and C is marked in E (open circles).

be associated with a reduction in the synchronization between the firing of spikes in dINs.

As is widely reported (Kiehn & Tresch, 2002; Connors & Long, 2004), electrical coupling effectively reduces membrane potential differences among connected neurons and can promote synchronous firing. The decrease in dIN firing reliability that we observed between dINs could therefore be related to increased differences in their membrane potential trajectories. We therefore examined membrane potential trajectories in recordings from pairs of dINs to see if electrical coupling block in 18-β-GA was associated with a reduction in their similarity, and so could account for the changes in synchronization of dIN firing and firing reliability. Apart from electrically coupled potentials, dINs receive on-cycle EPSPs from other dINs, mid-cycle IPSPs from cINs on the

opposite side of the spinal cord and some 'early-cycle' IPSPs from ipsilateral aINs during swimming. As well as variability in the strengths of these synaptic inputs, dIN spikes can also vary in amplitude and duration. For example, when the underlying depolarization is strong, dIN spikes decrease significantly in size (data not shown).

To provide a relatively simple comparison of overall membrane potential trajectories during swimming (including both spikes and synaptic drive), we used cross-correlation analyses of records from pairs of dINs, analysing 1–1.8 s per swimming episode. In each case, we used the peak value of the normalised cross-correlation coefficient as an index of the degree of similarity in membrane potential trajectory and the lag in the cross-correlation peak as an indication of the relative timing of trajectory changes in the two records.

Highly similar signals should have high cross-correlation peak values. Cross-correlation analyses in all six pairs showed that the peak coefficients were high early in each recording (0.87 ± 0.05), with short lags, confirming the similarity and synchronised nature of membrane trajectories in closely located dINs during normal swimming. Overall, peak coefficient values dropped to 0.68 ± 0.13 when electrical coupling block stabilised ($P = 0.027$, $n = 6$, paired *t*-test). In the two pairs where both dINs continued to fire reliable spikes (Fig. 8), peak coefficients remained relatively high throughout 18-β-GA application but they showed bigger variation in 18-β-GA (Fig. 9*A* and *E*). In the other four pairs where firing reliability dropped significantly in one or both dINs, there was a steady decline in correlation until peak coefficient values stabilised in parallel with the electrical coupling block (Fig. 9*C* and *E*). Membrane potential trajectories therefore became less similar following electrical coupling block. In contrast, the lag in the peak value changed little overall (from -0.8 ± 1.4 initially to -1.0 ± 1.9 ms once electrical coupling block stabilised, $P = 0.494$, $n = 6$, paired *t*-test, Fig. 9*F*). The relative timing of membrane potential trajectory changes in each neuron pair was therefore not related to electrical coupling strength (see below).
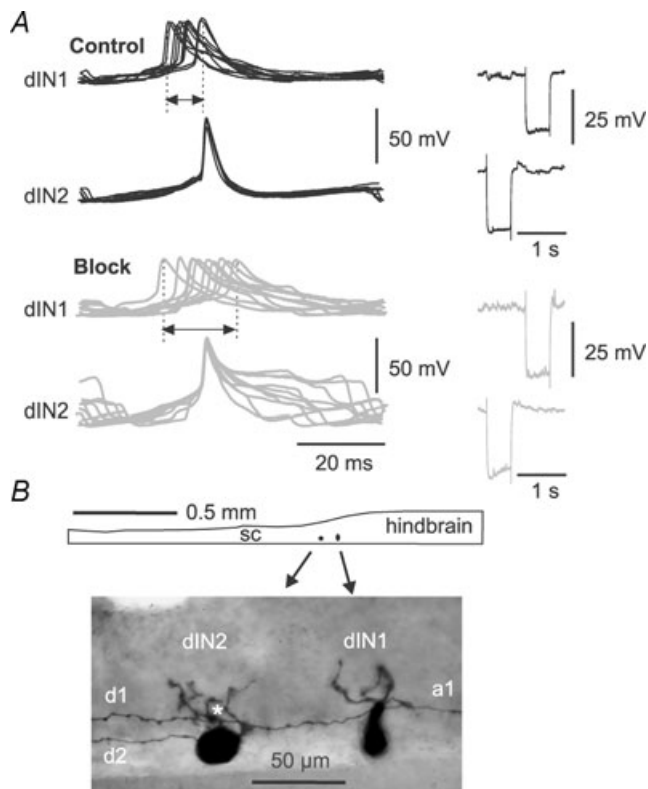
Relations between electrical coupling block, dIN activities and swimming changes

As outlined above, our experimental strategy involved using paired recordings to directly monitor electrical coupling strength during recordings. This allowed us to examine the relationship between a range of time series measurements to see if they followed parallel time courses and could therefore, plausibly, all be related to the same experimental manipulation: the block of electrical coupling between dINs.

Cross correlation analysis was applied between pairs of averaged time series measurements (made as

Figure 8. The firing of dINs in paired recordings became less synchronous when the electrical coupling was blocked
A, examples of less synchronous dIN firing in 18-β-GA. dIN spikes in 10 consecutive swimming cycles were lined up and superimposed to dIN2 spikes in control before 18-β-GA application and at electrical coupling block. In control, differences in timing are relatively small (range arrowed) and dIN1 firing is consistently earlier than dIN2. During coupling block, differences in timing are larger and some dIN1 spikes are later than dIN2 spikes. *B*, anatomy of the dINs in *A*. Diagram shows the location of dINs in caudal hindbrain/rostral spinal cord (sc). Dorsal is upwards. The photograph shows dIN anatomy in more detail: dIN1 has an ascending axon (a1) and a descending axon (d1) which contacts the basal dendrites of dIN2 (*) where electrical coupling may take place; dIN2 has only a descending axon (d2).

described above) for electrical coupling, dIN activity and swimming parameters (Fig. 10). Because there were only two pairs of dINs which continued to fire spikes reliably throughout 18-β-GA application, the spike timing difference measurements were not included in this analysis. The results (Table 1) revealed good pair-wise correlation (cross-correlation peak values > 0.75) between changes in the strength of electrical coupling, dIN firing reliability, similarity of membrane potential trajectories (cross correlation peak values from dIN paired recordings), swimming episode lengths, and ventral root burst durations. The relatively high values of cross-correlation peaks were coupled with no or very low lag values (Table 1), showing that the changes in all parameters occurred together. Although this result cannot confirm a causal link, it is therefore quite plausible that these changes were a direct consequence of the block of electrical coupling. In contrast, swimming cycle period and membrane trajectory cross-correlation lags (Fig. 9*F*) were only poorly correlated with all other measurements
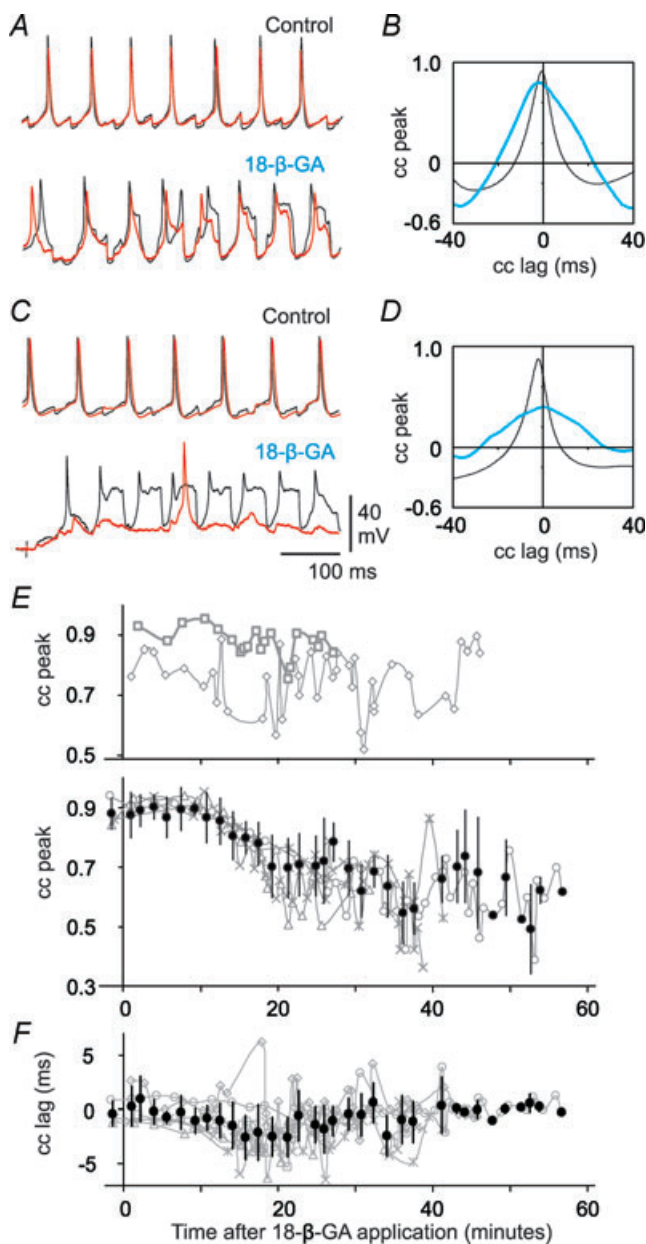

Figure 9. Membrane potential trajectories of dINs in swimming lose their similarity during 18-β-GA application

A, simultaneous recordings from 2 dINs (red and black traces overlain) firing reliable spikes throughout 18-β-GA application. Membrane trajectories are very similar in control. After electrical coupling block in 18-β-GA, this similarity is reduced. *B*, the cross-correlation (cc) between dIN recordings in A (black = control; blue = 18-β-GA). *C*, a second example of a dIN paired recording and *D*, its cross-correlation, where only one dIN fires reliable spikes during coupling block. The silent dIN (red trace) receives weak synaptic drive during coupling block. *E*, time series plots of cross-correlation peak values (cc peak) for 6 dIN pairs during swimming. Two dIN pairs continued to fire reliable spikes throughout 18-β-GA application; their correlation peak values change relatively little (top). In the other four pairs, one or both of the pair stopped firing reliably; their correlation peak values fall during 18-β-GA application (bottom). *F*, time series plot of cross-correlation lags; these change little during 18-β-GA application.
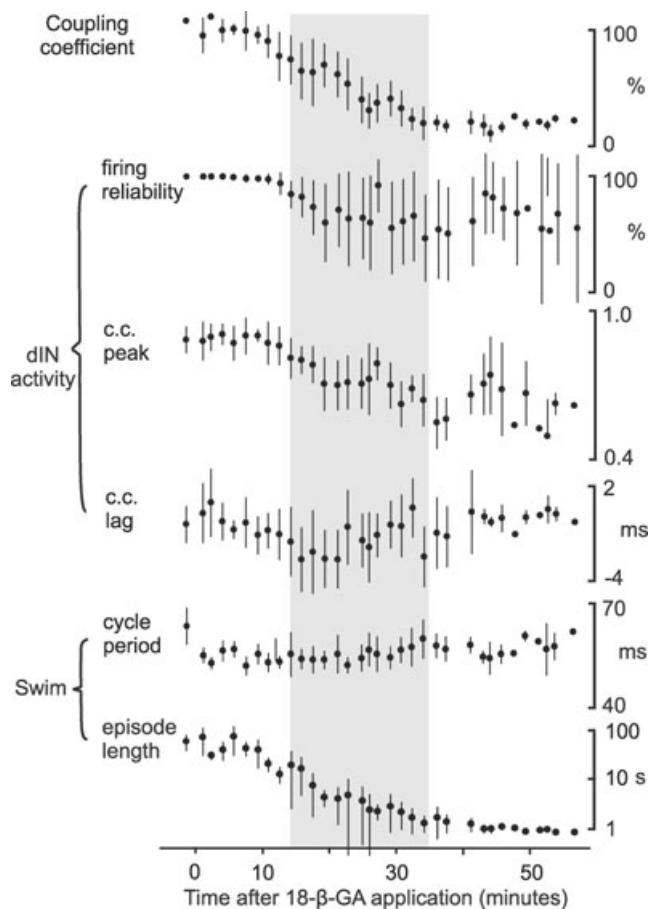
Figure 10. Summary of time series measurements

Values (mean ± s.d.) are for electrical coupling, dIN activities and swimming parameters in six paired recordings. Grey shading is between the mean times for the block to be detected and to reach stable block, respectively (see Fig. 6*B*).

Table 1. Cross correlation between averaged coupling coefficients, dIN activities and swimming parameters

		coupling ce	firing reliability	cc peak	cc lag	Episode length	VR duration
dIN activity	firing reliability	**0.79/0**	—	—	—	—	—
—	cc peak	**0.87/0**	**0.89/0**	—	—	—	—
	cc lag	−0.61/−9	−0.59/−8	−0.52/−8	—	—	—
swimming	Episode length	**0.84/0**	**0.76/0**	**0.76/−1**	−0.61/−9	—	—
	vr duration	**−0.94/0**	−0.73/0	**−0.84/0**	0.56/−6	**0.75/0**	—
	cycle period	−0.53/−5	−0.44/9	−0.54/−2	0.47/−2	−0.43/−4	0.6/2

Numbers before soliduses are cross-correlation peak values between each pair of averaged time series measurements. Numbers following soliduses are lags of correlation peak for each cross-correlation analysis. VR is ventral root and ce is coefficient. cc peak and cc lag are averaged measurements for the similarity between the two whole-cell recordings in each dIN pair. Cross-correlation peaks exceeding 0.75 are highlighted in bold.

suggesting that they were not significantly affected by the electrical coupling block (Table 1).

Discussion

In this paper, we present extensive evidence for widespread electrical coupling among the reticulospinal and spinal excitatory interneurons that drive the *Xenopus* tadpole swimming CPG, and suggest that this coupling significantly influences the ability of the swimming neuronal network to generate sustained activity.

In contrast to electrical coupling in the spinal cord of both lamprey (Parker, 2003) and zebrafish embryos (Saint-Amant & Drapeau, 2001), tadpole dINs are almost exclusively coupled to other dINs in the rostral spinal cord and caudal hindbrain region. This resembles the coupling in other brain areas where only interneurons of the same type are coupled (Gibson *et al.* 1999; Landisman *et al.* 2002; Blatow *et al.* 2003; Chu *et al.* 2003; Long *et al.* 2004). The proportion of dINs with electrical coupling (90%) is very high compared to other systems (Rekling & Feldman, 1997; Nolan *et al.* 1999; Rekling *et al.* 2000; Amitai *et al.* 2002; Long *et al.* 2002, 2004, 2005; Hinckley & Ziskind-Conhaim, 2006). Extensive gap junctional coupling was often suggested by dye-coupling experiments in developing nervous systems (e.g. neocortex; Peinado *et al.* 1993). Although the tadpoles we used in this study were just 2 days old, they have a functionally mature swimming circuit. This high incidence of coupling implies that every dIN in the swimming circuit will be coupled to many other dINs and the dINs are likely to function collectively as a group (of 150–200 on each side). This may partly explain why current injection into single hindbrain dINs can often start swimming (Li *et al.* 2006) and in some cases, strong negative current injection into single dINs may slow or stop swimming prematurely (W.-C.Li, unpublished observations). In contrast, our results suggest that there is no electrical coupling within or between other premotor interneuron groups. The exclusive and extensive coupling between dINs

therefore implies a role for electrical coupling that is specific to these excitatory interneurons. It should therefore be possible to explain some effects of blocking electrical coupling on swimming specifically in terms of changes in dIN coupling and activity. Additional effects on the final swimming output may also result from the electrical coupling described between motoneurons (Perrins & Roberts, 1995*a*,*b*).

The coupling strength of 8–9%, measured in paired whole-cell recordings from dIN somata, is very similar to that observed in other vertebrate rhythm generation systems (Rekling & Feldman, 1997; Nolan *et al.* 1999; Rekling *et al.* 2000; Saint-Amant & Drapeau, 2001; Hinckley & Ziskind-Conhaim, 2006). Given the widespread electrical coupling, dye coupling was surprising rare, observed with only 6% of dINs. This might be because most coupling between dINs involves their thin axons (<0.5 μm in diameter). Such coupling sites far away from the dIN somata might also explain the failure of intracellularly applied 18-β-GA to block dIN coupling. Axonal electrical coupling has been suggested as an effective and economical way to ensure reliable and highly synchronized firing among neuronal populations in comparison to chemical synapses or dendritic electrical synapses (Schmitz *et al.* 2001). We have argued here that electrical coupling between dINs can be strong enough to elicit action potentials in axons during swimming and may play a significant role in maintaining reliable firing in the dIN population (Fig. 3).

We manipulated electrical coupling using gap junction blockers. All gap junction blockers have some side effects which vary from preparation to preparation and complicate the interpretation of experimental results (e.g. Rozental *et al.* 2001; Rouach *et al.* 2003; Leznik & Llinas, 2005; Wang *et al.* 2006). Our initial screening of candidates led us to reject most in favour of 18-β-GA. Although 18-β-GA has side effects, we tried to evaluate these as possible confounding factors in interpreting the consequences of coupling block, which 18-β-GA produces effectively and which we monitored directly.

The tadpole swimming rhythm is very robust, and we should not expect subtle side-effects to produce the significant changes we observed. There were certainly no changes in the basic 'health' of cells: in RMP, or the ability to spike, or the threshold for spiking. There were changes in spike shape, but they appeared before the electrical coupling block when no significant changes in swimming patterns occurred. More importantly, they did not produce changes in EPSP size. There were no changes in the frequency of spontaneous PSPs, suggesting that the basic release mechanisms were not significantly affected. 18-β-GA produced similar short-term reduction in spike heights in the inhibitory interneurons. Its effects at the time of electrical coupling block on these neurons are not known but are likely to be similar to those observed on dINs. Further untested changes in inhibitory transmission remain possible, but previous experiments altering glycinergic transmission have always been associated with significant changes in cycle period. In 18-β-GA, the cycle period remained largely stable ($\sim$5% change), and 'mid cycle' inhibition was still clearly present in the neurons that had distinct synaptic drive. We cannot rule out other untested side-effects which had the same time course as coupling block and were therefore not distinguished by the detailed cross-correlation analysis. However the interpretation that follows assumes that the observed effects on swimming and dIN activity result from the one large and significant change that was measured: the substantial reduction of coupling strength.

Application of 18-β-GA produced significant changes in the activity of dINs during swimming; broadly, their firing became less reliable, so that half of dINs failed to fire on many swimming cycles, and their activity became increasingly divergent, with less synchronised firing and larger differences in synaptic drive. Our sinusoidal current injection tests showed that signals below 10 Hz are optimally transferred between dINs. The action potentials of dINs are unusually wide (Li *et al.* 2006) and widen significantly further during swimming (unpublished observation). This suggests both slow rhythmic synaptic potentials generated in swimming and broad dIN action potentials are well suited temporally to be coupled to other dINs. This could help explain why the activity of dINs during swimming is remarkably reliable and similar: a single wide spike on each swimming cycle and very similar trajectories of synaptic drive. When the coupling is blocked, differences in dIN synaptic drives emerge. Those dINs with weaker drives stop firing and dIN firing synchrony loosens. In line with our observation of the difficulty in stopping dIN firing during normal swimming (Fig. 3), these results suggest that the electrical coupling plays an important role in ensuring highly reliable and common activity across the dIN population.

Does the common pattern of activity in dINs in turn influence the form of the final motor output during swimming? Swift *Xenopus* tadpole swimming is controlled by near-synchronous firing of neighbouring motoneurons. Electrical coupling between motoneurons may contribute to this synchronized firing (Perrins & Roberts, 1995*a*,*b*). However, motoneuron firing is driven by a strongly phasic on-cycle excitation which results from the closely synchronised firing in the dIN population. The block of electrical coupling among dINs that we suggest contributes to loosening of this synchronization of dIN firing will result in less precisely timed excitation to motoneurons and may well contribute to the observed prolonging of ventral root bursts.

The shortening of swimming episodes that accompanies block of dIN electrical coupling suggests that the coupling may significantly influence the mechanisms that sustain swimming. We recently identified positive feedback between dINs as being critical for persistent swimming (Li *et al.* 2006). This positive feedback relies on the ascending axonal branches of half of the dIN population in the hindbrain to produce NMDAR mediated excitation that summates from cycle to cycle, outlasting early-cycle and mid-cycle inhibition. Some dINs then fire on rebound following reciprocal, mid-cycle inhibition and carry the swimming activity into another cycle. Unlike conventional rebound firing, occurring from the resting membrane potential, dINs need a background depolarisation for rebound firing and the NMDAR mediated feedback excitation is thus critically important in swimming maintenance (Li *et al.* 2006). One effect of 18-β-GA block of electrical coupling is apparently to prevent an even distribution of synaptic excitation among dINs. Any dINs which receive strong chemical EPSPs will continue firing once per cycle because of their single-firing properties (Li *et al.* 2006). However, any dINs receiving weak EPSPs will stop firing (Figs 7 and 9). The consequent drop in the number of dIN spikes on each swimming cycle in 18-β-GA will further weaken the long-lasting NMDAR feedback excitation in dINs. This weakened depolarisation in dINs will then cause rebound firing to fail in progressively more dINs. At the same time, the ability of axo-axonal coupling to help support spiking (Fig. 3, also see discussion above) will also be reduced or lost. If this interpretation is correct, the combined result will be for swimming to stop prematurely. The ability of the swimming circuit to generate sustained rhythm is not significantly affected by removing most of the spinal cord and therefore its motoneurons (Li *et al.* 2006), suggesting the contribution of motoneurons to swimming maintenance is minimal. The effects of 18-β-GA on maintenance of the swimming rhythm are thus unlikely to result from the block of electrical coupling between motoneurons. The brief swimming that remains may result from excitation produced by the swimming initiation pathway (Li *et al.* 2003), which can last for a few hundred milliseconds after stimulation.

By basing our investigation on the hatchling *Xenopus* tadpole where we have detailed knowledge about the locomotor network, we have been able to take the unusual step of examining the importance of electrical coupling at the level of a whole neuronal system. Our results highlight different possible roles for electrical coupling in rhythm-generating circuits. Synchronization of neuronal activity, often seen as locked firing frequency and phase across neurons (Rekling & Feldman, 1997; Gibson *et al.* 1999; Prime *et al.* 1999; Moortgat *et al.* 2000*a,b*; Leznik & Llinas, 2005), is one direct effect of electrical coupling. However, as we show here for excitatory premotor interneurons driving locomotion, coupling at the inter-neuron level may have a deeper role in supporting robust firing in a whole population. Although electrical coupling has been found in many vertebrate spinal cord and brain-stem preparations, only its role in synchronizing neuronal firing was well established (Moortgat *et al.* 2000*a*; Kiehn & Tresch, 2002). The roles hindbrain and spinal excitatory premotor interneurons play in locomotion maintenance in other vertebrates are still poorly understood. Whether or not the electrical coupling found between them (Christensen, 1983; Saint-Amant & Drapeau, 2001; Parker, 2003; Hinckley & Ziskind-Conhaim, 2006) plays a similar role to the one suggested in the tadpole remains to be examined.

References

Alvarez VA, Chow CC, Van Bockstaele EJ & Williams JT (2002). Frequency-dependent synchrony in locus ceruleus: role of electrotonic coupling. *Proc Natl Acad Sci U S A* **99**, 4032–4036.

Amitai Y, Gibson JR, Beierlein M, Patrick SL, Ho AM, Connors BW & Golomb D (2002). The spatial dimensions of electrically coupled networks of interneurons in the neocortex. *J Neurosci* **22**, 4142–4152.

Asghar AU, Cilia La Corte PF, LeBeau FE, Al Dawoud M, Reilly SC, Buhl EH, Whittington MA & King AE (2005). Oscillatory activity within rat substantia gelatinosa *in vitro*: a role for chemical and electrical neurotransmission. *J Physiol* **562**, 183–198.

Ballantyne D, Andrzejewski M, Muckenhoff K & Scheid P (2004). Rhythms, synchrony and electrical coupling in the locus coeruleus. *Respir Physiol Neurobiol* **143**, 199–214.

Blatow M, Rozov A, Katona I, Hormuzdi SG, Meyer AH, Whittington MA, Caputi A & Monyer H (2003). A novel network of multipolar bursting interneurons generates theta frequency oscillations in neocortex. *Neuron* **38**, 805–817.

Blenkinsop TA & Lang EJ (2006). Block of inferior olive gap junctional coupling decreases Purkinje cell complex spike synchrony and rhythmicity. *J Neurosci* **26**, 1739–1748.

Bou-Flores C & Berger AJ (2001). Gap junctions and inhibitory synapses modulate inspiratory motoneuron synchronization. *J Neurophysiol* **85**, 1543–1551.

Chang Q, Gonzalez M, Pinter MJ & Balice-Gordon RJ (1999). Gap junctional coupling and patterns of connexin expression among neonatal rat lumbar spinal motor neurons. *J Neurosci* **19**, 10813–10828.

Christensen BN (1983). Distribution of electrotonic synapses on identified lamprey neurons: a comparison of a model prediction with an electron microscopic analysis. *J Neurophysiol* **49**, 705–716.

Christie MJ, Williams JT & North RA (1989). Electrical coupling synchronizes subthreshold activity in locus coeruleus neurons in vitro from neonatal rats. *J Neurosci* **9**, 3584–3589.

Chu Z, Galarreta M & Hestrin S (2003). Synaptic interactions of late-spiking neocortical neurons in layer 1. *J Neurosci* **23**, 96–102.

Connors BW & Long MA (2004). Electrical synapses in the mammalian brain. *Annu Rev Neurosci* **27**, 393–418.

Cullheim S, Kellerth JO & Conradi S (1977). Evidence for direct synaptic interconnections between cat spinal α-motoneurons via the recurrent axon collaterals: a morphological study using intracellular injection of horseradish peroxidase. *Brain Res* **132**, 1–10.

Dai Y, Jones KE, Fedirchuk B, McCrea DA & Jordan LM (2002). A modelling study of locomotion-induced hyperpolarization of voltage threshold in cat lumbar motoneurones. *J Physiol* **544**, 521–536.

Draguhn A, Traub RD, Schmitz D & Jefferys JG (1998). Electrical coupling underlies high-frequency oscillations in the hippocampus in vitro. *Nature* **394**, 189–192.

Friedman D & Strowbridge BW (2003). Both electrical and chemical synapses mediate fast network oscillations in the olfactory bulb. *J Neurophysiol* **89**, 2601–2610.

Fulton BP, Miledi R & Takahashi T (1980). Electrical synapses between motoneurons in the spinal cord of the newborn rat. *Proc R Soc Lond B Biol Sci* **208**, 115–120.

Gibson JR, Beierlein M & Connors BW (1999). Two networks of electrically coupled inhibitory neurons in neocortex. *Nature* **402**, 75–79.

Grinnell AD (1966). A study of the interaction between motoneurones in the frog spinal cord. *J Physiol* **182**, 612–648.

Hinckley CA & Ziskind-Conhaim L (2006). Electrical coupling between locomotor-related excitatory interneurons in the mammalian spinal cord. *J Neurosci* **26**, 8477–8483.

Kiehn O & Tresch MC (2002). Gap junctions and motor behavior. *Trends Neurosci* **25**, 108–115.

Krawitz S, Fedirchuk B, Dai Y, Jordan LM & McCrea DA (2001). State-dependent hyperpolarization of voltage threshold enhances motoneurone excitability during fictive locomotion in the cat. *J Physiol* **532**, 271–281.

Landisman CE, Long MA, Beierlein M, Deans MR, Paul DL & Connors BW (2002). Electrical synapses in the thalamic reticular nucleus. *J Neurosci* **22**, 1002–1009.

Leznik E & Llinas R (2005). Role of gap junctions in synchronized neuronal oscillations in the inferior olive. *J Neurophysiol* **94**, 2447–2456.

Li W-C, Soffe SR, Wolf E & Roberts A (2006). Persistent responses to brief stimuli: feedback excitation among brainstem neurons. *J Neurosci* **26**, 4026–4035.

Li WC, Higashijima S, Parry DM, Roberts A & Soffe SR (2004*a*). Primitive roles for inhibitory interneurons in developing frog spinal cord. *J Neurosci* **24**, 5840–5848.

Li WC, Perrins R, Soffe SR, Yoshida M, Walford A & Roberts A (2001). Defining classes of spinal interneuron and their axonal projections in hatchling *Xenopus laevis* tadpoles. *J Comp Neurol* **441**, 248–265.

Li WC, Soffe SR & Roberts A (2002). Spinal inhibitory neurons that modulate cutaneous sensory pathways during locomotion in a simple vertebrate. *J Neurosci* **22**, 10924–10934.

Li WC, Soffe SR & Roberts A (2003). The spinal interneurons and properties of glutamatergic synapses in a primitive vertebrate cutaneous flexion reflex. *J Neurosci* **23**, 9068–9077.

Li WC, Soffe SR & Roberts A (2004*b*). Glutamate and acetylcholine corelease at developing synapses. *Proc Natl Acad Sci U S A* **101**, 15488–15493.

Logan SD, Pickering AE, Gibson IC, Nolan MF & Spanswick D (1996). Electrotonic coupling between rat sympathetic preganglionic neurones in vitro. *J Physiol* **495**, 491–502.

Long MA, Deans MR, Paul DL & Connors BW (2002). Rhythmicity without synchrony in the electrically uncoupled inferior olive. *J Neurosci* **22**, 10898–10905.

Long MA, Jutras MJ, Connors BW & Burwell RD (2005). Electrical synapses coordinate activity in the suprachiasmatic nucleus. *Nat Neurosci* **8**, 61–66.

Long MA, Landisman CE & Connors BW (2004). Small clusters of electrically coupled neurons generate synchronous rhythms in the thalamic reticular nucleus. *J Neurosci* **24**, 341–349.

Mazza E, Nunez-Abades PA, Spielmann JM & Cameron WE (1992). Anatomical and electrotonic coupling in developing genioglossal motoneurons of the rat. *Brain Res* **598**, 127–137.

Moortgat KT, Bullock TH & Sejnowski TJ (2000*a*). Gap junction effects on precision and frequency of a model pacemaker network. *J Neurophysiol* **83**, 984–997.

Moortgat KT, Bullock TH & Sejnowski TJ (2000*b*). Precision of the pacemaker nucleus in a weakly electric fish: network versus cellular influences. *J Neurophysiol* **83**, 971–983.

Nolan MF, Logan SD & Spanswick D (1999). Electrophysiological properties of electrical synapses between rat sympathetic preganglionic neurones in vitro. *J Physiol* **519**, 753–764.

Parker D (2003). Variable properties in a single class of excitatory spinal synapse. *J Neurosci* **23**, 3154–3163.

Peinado A, Yuste R & Katz LC (1993). Extensive dye coupling between rat neocortical neurons during the period of circuit formation. *Neuron* **10**, 103–114.

Perrins R & Roberts A (1995*a*). Cholinergic and electrical motoneuron-to-motoneuron synapses contribute to on-cycle excitation during swimming in *Xenopus* embryos. *J Neurophysiol* **73**, 1005–1012.

Perrins R & Roberts A (1995*b*). Cholinergic and electrical synapses between synergistic spinal motoneurones in the *Xenopus laevis* embryo. *J Physiol* **485**, 135–144.

Prime L, Pichon Y & Moore LE (1999). N-Methyl-D-aspartate-induced oscillations in whole cell clamped neurons from the isolated spinal cord of *Xenopus laevis* embryos. *J Neurophysiol* **82**, 1069–1073.

Rash JE, Dillman RK, Bilhartz BL, Duffy HS, Whalen LR & Yasumura T (1996). Mixed synapses discovered and mapped throughout mammalian spinal cord. *Proc Natl Acad Sci U S A* **93**, 4235–4239.

Rekling JC & Feldman JL (1997). Bidirectional electrical coupling between inspiratory motoneurons in the newborn mouse nucleus ambiguus. *J Neurophysiol* **78**, 3508–3510.

Rekling JC, Shao XM & Feldman JL (2000). Electrical coupling and excitatory synaptic transmission between rhythmogenic respiratory neurons in the preBotzinger complex. *J Neurosci* **20**, RC113.

Roberts A (2000). Early functional organization of spinal neurons in developing lower vertebrates. *Brain Res Bull* **53**, 585–593.

Roberts A & Alford ST (1986). Descending projections and excitation during fictive swimming in *Xenopus* embryos: neuroanatomy and lesion experiments. *J Comp Neurol* **250**, 253–261.

Roberts A & Clarke JDW (1982). The neuroanatomy of an amphibian embryo spinal cord. *Phil Trans Roy Soc* **296**, 195–212.

Roopun AK, Middleton SJ, Cunningham MO, LeBeau FEN, Bibbig A, Whittington MA & Traub RD (2006). A $\beta2$-frequency (20–30 Hz) oscillation in nonsynaptic networks of somatosensory cortex. *Proc Natl Acad Sci U S A* **103**, 15646–15650.

Rouach N, Segal M, Koulakoff A, Giaume C & Avignone E (2003). Carbenoxolone blockade of neuronal network activity in culture is not mediated by an action on gap junctions. *J Physiol* **553**, 729–745.

Rozental R, Srinivas M & Spray DC (2001). How to close a gap junction channel. Efficacies and potencies of uncoupling agents. *Methods Mol Biol* **154**, 447–476.

Saint-Amant L & Drapeau P (2001). Synchronization of an embryonic network of identified spinal interneurons solely by electrical coupling. *Neuron* **31**, 1035–1046.

Schmitz D, Schuchmann S, Fisahn A, Draguhn A, Buhl EH, Petrasch-Parwez E, Dermietzel R, Heinemann U & Traub RD (2001). Axo-axonal coupling. A novel mechanism for ultrafast neuronal communication. *Neuron* **31**, 831–840.

Sinfield JL & Collins DR (2006). Induction of synchronous oscillatory activity in the rat lateral amygdala in vitro is dependent on gap junction activity. *Eur J Neurosci* **24**, 3091–3095.

Srinivas M & Spray DC (2003). Closure of gap junction channels by arylaminobenzoates. *Mol Pharmacol* **63**, 1389–1397.

Traub RD, Pais I, Bibbig A, LeBeau FE, Buhl EH, Hormuzdi SG, Monyer H & Whittington MA (2003). Contrasting roles of axonal (pyramidal cell) and dendritic (interneuron) electrical coupling in the generation of neuronal network oscillations. *Proc Natl Acad Sci U S A* **100**, 1370–1374.

Tresch MC & Kiehn O (2000). Motor coordination without action potentials in the mammalian spinal cord. *Nat Neurosci* **3**, 593–599.

Tresch MC & Kiehn O (2002). Synchronization of motor neurons during locomotion in the neonatal rat: predictors and mechanisms. *J Neurosci* **22**, 9997–10008.

Urbano FJ, Leznik E & Llinas RR (2007). Modafinil enhances thalamocortical activity by increasing neuronal electrotonic coupling. *Proc Natl Acad Sci U S A* **104**, 12554–12559.

Van Der Giessen RS, Koekkoek SK, van Dorp S, De Gruijl JR, Cupido A, Khosrovani S, Dortland B, Wellershaus K, Degen J, Deuchars J, Fuchs EC, Monyer H, Willecke K, De Jeu MTG & De Zeeuw CI (2008). Role of olivary electrical coupling in cerebellar motor learning. *Neuron* **58**, 599–612.

Walton KD & Navarrete R (1991). Postnatal changes in motoneurone electrotonic coupling studied in the in vitro rat lumbar spinal cord. *J Physiol* **433**, 283–305.

Wang D, Grillner S & Wallen P (2006). Effects of flufenamic acid on fictive locomotion, plateau potentials, calcium channels and NMDA receptors in the lamprey spinal cord. *Neuropharmacol* **51**, 1038–1046.

Westerfield M & Frank E (1982). Specificity of electrical coupling among neurons innervating forelimb muscles of the adult bullfrog. *J Neurophysiol* **48**, 904–913.

Zsiros V, Aradi I & Maccaferri G (2007). Propagation of postsynaptic currents and potentials via gap junctions in GABAergic networks of the rat hippocampus. *J Physiol* **578**, 527–544.

Author contributions

The experiments were carried out in the University of Bristol by Dr Wen-Chang Li. All three authors contributed to the conception of the hypothesis, design of the experiments, analysis and interpretation of data and writing of the manuscript.

Author's present address

W.-C. Li: School of Biology, University of St Andrews, Bute Medical Building, Fife KY16 9TS, Scotland, UK.